SCIENTIFIC REPORTS

OPEN

SUBJECT AREAS:
COORDINATION CHEMISTRY
MAGNETIC PROPERTIES AND MATERIALS

Received
23 October 2014

Accepted
17 November 2014

Published
11 December 2014

Correspondence and requests for materials should be addressed to P.S. (paolo.santini@unipr.it)

Molecular nanomagnets with switchable coupling for quantum simulation

Alessandro Chiesa[1,2], George F. S. Whitehead[3], Stefano Carretta[1], Laura Carthy[3], Grigore A. Timco[3], Simon J. Teat[4], Giuseppe Amoretti[1], Eva Pavarini[2,5], Richard E. P. Winpenny[3] & Paolo Santini[1]

[1]Dipartimento di Fisica e Scienze della Terra, Università di Parma, Parco Area delle Scienze 7/a, 43124 Parma, Italy, [2]Institute for Advanced Simulation, Forschungszentrum Jülich, 52425 Jülich, Germany, [3]School of Chemistry and Photon Science Institute, University of Manchester, Oxford Road, Manchester M13 9PL, United Kingdom, [4]Advanced Light Source, Lawrence Berkeley Laboratory, MS2-400 Berkeley, California 94720, USA, [5]JARA High-Performance Computing.

Molecular nanomagnets are attractive candidate qubits because of their wide inter- and intra-molecular tunability. Uniform magnetic pulses could be exploited to implement one- and two-qubit gates in presence of a properly engineered pattern of interactions, but the synthesis of suitable and potentially scalable supramolecular complexes has proven a very hard task. Indeed, no quantum algorithms have ever been implemented, not even a proof-of-principle two-qubit gate. Here we show that the magnetic couplings in two supramolecular {Cr_7Ni}-Ni-{Cr_7Ni} assemblies can be chemically engineered to fit the above requisites for conditional gates with no need of local control. Microscopic parameters are determined by a recently developed many-body *ab-initio* approach and used to simulate quantum gates. We find that these systems are optimal for proof-of-principle two-qubit experiments and can be exploited as building blocks of scalable architectures for quantum simulation.

In the last few years there have been great advances in the domain of experimental implementation of quantum information processing[1]. A major objective is the construction of quantum simulators (QSs), yielding massively increased computational power in simulating quantum systems. Envisioned 30 years ago by Richard Feynman[2], QSs are now attracting considerable interest in many areas of physics. The huge Hilbert space of a general quantum system is encoded and stored efficiently on a QS using the wavefunctions of its qubits, whose dynamics can be controlled so as to mimic the evolution of the target system[3,4]. Many physical properties can be extracted in polynomial time by operating such a device and by performing measurements according to specific algorithms[5].

Molecular nanomagnets (MNMs)[6] have been proposed as promising candidates for both spintronics[7–9] and quantum information processing (QIP)[10–15]. The attractiveness of MNMs stems from their wide tunability, both at the intermolecular and at the intramolecular level. One-qubit operations have already been performed on ensembles[16–18], and the observed coherence times are long enough to implement more complex algorithmic sequences. In order to implement such sequences, the most direct way would be to use external magnetic fields varying in time and from qubit to qubit and an external tool to switch on and off the qubit-qubit couplings locally for two-qubit gates. This represents an extremely tough experimental challenge.

A much less demanding approach is to use uniform magnetic fields to induce the required time evolution of the register, by exploiting auxiliary states and the structure of intermolecular interactions[19–21]. This quantum simulation scheme[21] is based on two classes of MNMs that play two distinct roles: effective $S = 1/2$ spins are used to encode the qubits, whereas interposed complexes with a singlet ground state are used as switches of the effective qubit-qubit interaction. In particular, by an appropriate topology and hierarchy of exchange couplings between different molecular units, it would be possible to use uniform pulses to switch on and off intermolecular interactions, thus implementing two-qubit gates and quantum simulation algorithms[21]. However, the engineering of potentially scalable supramolecular complexes fitting these requisites has proven a very hard chemical task.

Here we show that new supramolecular assemblies have the correct characteristics to implement one- and two-qubits gates with uniform magnetic fields, i.e., with no need of local control. The magnetic couplings are engineered by coordination chemistry and several variants with different geometry are obtained. These two-qubits units are optimal for proof-of-principle experiments and can be exploited as building blocks of scalable architectures for quantum simulation.

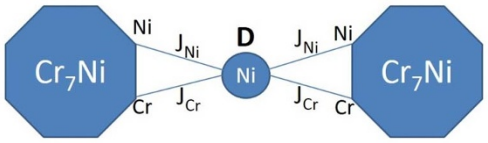

Figure 1 | Scheme of a pair of {Cr_7Ni} rings, linked by a Ni^{2+}ion. The effective isotropic and axial Ni-ring couplings are given by $J_{iso} = 1.13J_{Cr} - 0.63J_{Ni}$ and $J_{an} = 0.14J_{Cr} - 0.10J_{Ni}$, respectively (see Eqs. (1) and (2)).

Results

The $S = 1/2$ MNMs have the chemical formula [^{n}Pr_2NH_2][$Cr_7NiF_8(O_2C^tBu)_{16}$)] **1** (where O_2C^tBu = pivalate); these antiferromagnetically-coupled rings[23,24] behave at low temperature as effective $S = 1/2$ spins and show long coherence times[24], and are therefore excellent candidates for the role of qubits[11]. As a switch we propose a monometallic Ni^{2+} complex, exploiting the axial anisotropy of this $S = 1$ spin to turn on and off the effective qubit-qubit interaction. A sketch of the here-proposed systems is shown in Figure 1.

As we will show below, if the Ni ion is frozen in the ground state, the coupling of each ring with the switch merely renormalizes the external magnetic field and single-qubit gates can be implemented. Conversely, two-qubit gates are performed by temporarily bringing the Ni ion to an excited state by a microwave pulse. This scheme requires that the energy of the excited state of the switch is much larger than the qubit-switch coupling. However, this coupling must be large-enough to ensure that the excitation energy of the switch is sufficiently dependent on the state of the qubits to enable conditional dynamics. This requires a chemical engineering of the qubit-switch bond to obtain a suitable hierarchy of the parameters.

Synthesis and structural studies. To match the schematic structure (Figure 1) in a supramolecule we introduce an N-donor ligand onto the backbone of the {Cr_7Ni} ring by reaction of **1** with a carboxylate containing an N-heterocycle, for example *iso*-nicotinic acid (H_2OC-py) or pyridazine-4-carboxylic acid (H_2O-pd). The incoming acid displaces one pivalate to produce [^{n}Pr_2NH_2][$Cr_7NiF_8(O_2C^tBu)_{15}$(O_2C-py)] **2** or [^{n}Pr_2NH_2][$Cr_7NiF_8(O_2C^tBu)_{15}(O_2C$-pd)] **3** respectively. The following assemblies have been prepared, and show either *cis* or *trans* arrangements of the rings about the central nickel: [*cis*-(**2**)$_2$-Ni$(NO_3)_2(H_2O)_2$] **4**; [*cis*-(**3**)$_2$-Ni(hfac)$_2$] **5**; [*trans*-(**2**)$_2$-Ni(acac)$_2$] **6**; [*trans*-(**2**)$_2$-Ni(hfac)$_2$] **7**; [*trans*-(**2**)$_2$-Ni(tfac)$_2$] **8**; (where acac = acetylacetonate; Hhfac = 1,1,1,5,5,5-hexafluoroacetylacetonate; tfac = 1,1,1-trifluoroacetylacetonate). These five compounds have been structurally characterized (Figure 2). See Supplementary Information for more details.

The compounds all contain two {Cr_7Ni} rings disposed about a central nickel(II) switch (Figure 2). The structural parameters within the individual {Cr_7Ni} rings are unchanged between the compounds, however the coordination geometries at the central Ni-site varies between the compounds (Table 1). Compounds **4** and **5** contain a *cis* arrangement of the N-donors derived from the substituted rings and in both cases the central Ni site lies on a two-fold rotation axis. In **6** – **8** the pyridine donors are arranged *trans*; for **7** and **8** the Ni site sits on an inversion centre, while for **6** the Ni is not on any symmetry element. In each case the Ni site is six-coordinate, with four sites occupied by O-donors, derived from β-diketonates in **5** – **8** and two monodentate nitrates and two water molecules in **4**. The chemistry allows us to modify the crystal environment of the Ni-switch moving from *cis* to *trans* geometries, and this influences the Ni anisotropy and the Ni-ring coupling. If we consider the two *cis*-compounds, the Ni-N distance is noticeable longer in **5** than in **4**, suggesting the strength of the Ni-ring coupling will be weaker in **5** than in **4**. The variation in the *trans*-compounds is perhaps more subtle; the Ni-N bond length is very slightly longer in **6**. The bond angles are all close to those expected for a regular octahedral coordination geometry, with the greatest variation found for compound **6**, which is the only molecule where the Ni is not on a symmetry element. Within each

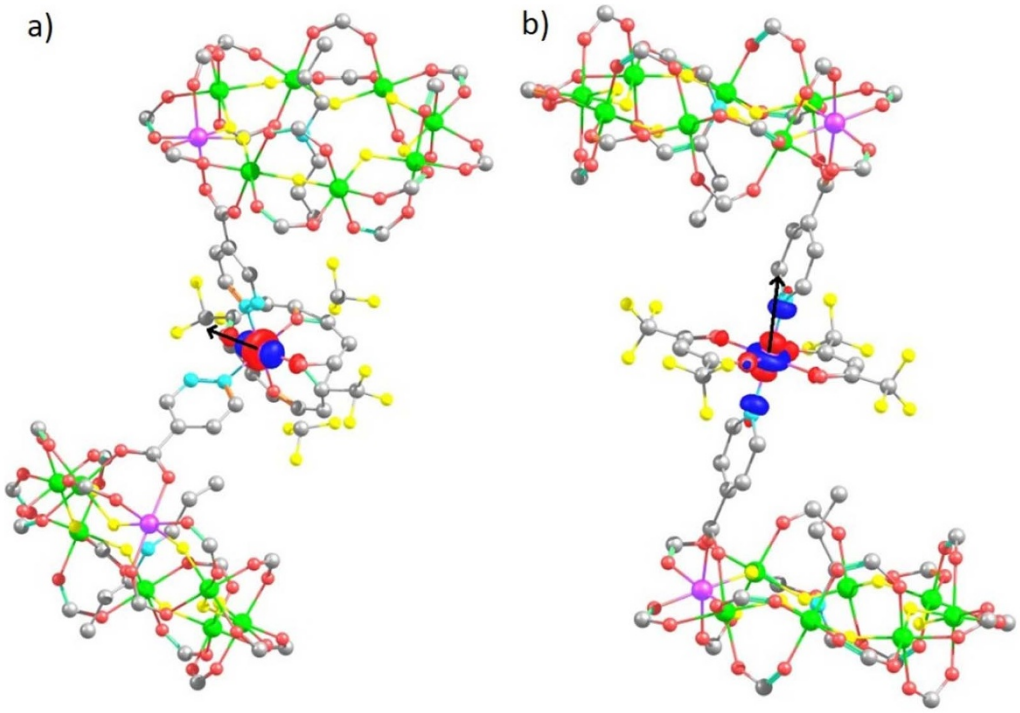

Figure 2 | Molecular structures determined from X-ray data for a) 5 and b) 7. The planes of the two rings are parallel in 7, while they are not in 5. The localized highest energy *3d* orbital on the central ion obtained by *ab-initio* calculations is also shown. The black arrows indicate the *z* direction in Eq. (1), determined by diagonalization of the zero-field-splitting tensor calculated *ab-initio*. In the figure, H atoms and CH_3 groups on the rings are not shown for clarity, O are red, F are yellow, C are grey, N blue, Cr green and Ni violet.

family of compounds, the Ni-ring coupling is also controlled by the chemical substitution $CF_3 \rightarrow CH_3$ close to the Ni-ring bond. In addition, we can envisage connecting some of these elementary units in order to obtain chains of qubits.

Many-body ab-initio calculations. Direct physical measurements of ring-Ni exchange interactions are very difficult as variable temperature susceptibility measurements are dominated by the exchange interactions within rings, masking the ring-Ni interaction. Very low temperature magnetization measurements might reveal the ring-Ni exchange, however such measurements are very challenging. Given that our conclusions are grounded on the hierarchy of the different parameters and not on their precise values, we have investigated the possibility of implementing quantum gates by performing an *ab-initio* study of these compounds. Calculations for these huge molecules (several hundreds atoms) are very time consuming. We employ the NWChem quantum chemistry code[25], which is optimized to exploit the power of modern massively parallel supercomputers. These calculations are based on a novel and flexible approach which has already been successfully applied to determine the spin Hamiltonians of three prototype MNMs, including **1**[22]. Differently from other schemes, such as those based on hybrid functionals or LDA+U[26–28], strong correlation effects are not accounted for at a static mean field level. They are explicitly included in a generalized Hubbard model[29], which is constructed using localized Boys orbitals[30] to describe the 3*d* electrons of the transition metal ions[31]. The model accounts for both electron-transfer effects, via the hopping integrals, and strong electron-electron correlations, controlled by the screened Coulomb integrals. The hopping integrals are obtained at the end of a self-consistent DFT run, performed in Local Density Approximation (LDA). In a subsequent step, the screened Coulomb integrals are also calculated self-consistently by means of the constrained LDA method[32]. This leads to a molecule-specific generalized Hubbard model. Finally, the spin Hamiltonian is obtained by means of a canonical transformation[33] applied to such a Hubbard model. In this way, no assumption on the form of this Hamiltonian is needed and all the interactions are deduced systematically, including the subtle anisotropic terms. For the present class of compounds, we obtain the following microscopic spin Hamiltonian:

$$H_{micro} = \sum_{i=1}^{2} \left(J_{Ni} \mathbf{S} \cdot \mathbf{s}_{Ni}^{i} + J_{Cr} \mathbf{S} \cdot \mathbf{s}_{Cr}^{i} \right) + \mathbf{S} \cdot \underline{\mathbf{D}} \cdot \mathbf{S} + \mu_B \mathbf{B} \cdot \underline{\mathbf{g}}^{Ni} \cdot \mathbf{S} + \sum_{i=1}^{2} H_{ring}(i) \,, \quad (1)$$

where the first term describes the exchange coupling between the two $\{Cr_7Ni\}$ rings and the Ni-switch, and $\underline{\mathbf{D}}$ is the zero field splitting tensor of the Ni ion (Figure 1). We indicate with capital letters (S) the spin of the Ni-switch and with lowercase letters those belonging to the rings ($\mathbf{s}_{Ni}^{1,2}$, $\mathbf{s}_{Cr}^{1,2}$). The last term describes the intra-ring Hamiltonian which has been determined from neutron spectroscopy[23], torque magnetometry[34] and electron paramagnetic resonance[15]. The parameters of H_{ring} inferred from experiments are in agreement with those calculated from first principles by means of the present approach[22].

The exchange constants J_{Ni} and J_{Cr} are the sum of a ferromagnetic (FM) screened Coulomb exchange contribution J^{CE} and a super-exchange term J^{SE}, which contains both FM and AFM contributions. It is important to point out that the Ni-ring superexchange coupling, although very small ($J^{SE} \sim 10$ μeV), can be reliably obtained by means of the present approach. Indeed, the value of J^{SE} depends on the ratio between the square of the hopping integrals (of the order of meV) and the screened Coulomb terms (~eV), both very large in comparison with numerical errors. The screened value of J^{CE} is in this case too small to be reliably determined with the constrained LDA approach. Nevertheless, a reasonable estimate can be obtained by assuming that the bare Coulomb exchange integrals are reduced by the same screening-factor determined *ab-initio* for **1** in reference 22. Finally, $\underline{\mathbf{D}}$ and the small anisotropy of the $\underline{\mathbf{g}}^{Ni}$ tensor originate from the combined action of crystal-field and spin-orbit interactions. We determine the full tensors and we diagonalize them in order to find the principal anisotropy axes.

Effective low-energy Hamiltonian. Since the interactions of each ring with the Ni-switch are much weaker than the intra-ring couplings, the microscopic Hamiltonian H_{micro} (Eq. (1)) can be projected in the subspace in which the two rings are in the ground doublets. These are described by effective spins $T = 1/2$, thus obtaining:

$$\begin{aligned} H_S = {} & J_{iso} \mathbf{S} \cdot \sum_{i=1}^{2} \mathbf{T}^i + J_{an} \sum_{i=1}^{2} \left(2 S_z T_{z_i}^i - S_x T_{x_i}^i - S_y T_{y_i}^i \right) \\ & + D \left[S_Z^2 - \frac{S(S+1)}{3} \right] + E \left(S_x^2 - S_y^2 \right) + \mu_B \mathbf{B} \cdot \underline{\mathbf{g}}^{Ni} \cdot \mathbf{S} + \mu_B \mathbf{B} \cdot \sum_{i=1}^{2} \underline{\mathbf{g}}^{Ni} \cdot \mathbf{T}^i \end{aligned} \quad (2)$$

where S_α and T_α^i indicate, respectively, the components of the spin of the Ni-switch and of each ring, *z, x, y*, are the principal anisotropy axes of the Ni ion and z_i, x_i, y_i, are the principal axes of the two rings. D and E are axial and rhombic zero-field-splitting parameters. The last terms describe the Zeeman interaction with an external field ***B***. The effective exchange parameters can be then deduced from the microscopic parameters calculated *ab-initio*: we find that $J_{iso} = 1.13\ J_{Cr} - 0.63\ J_{Ni}$ and $J_{an} = 0.14\ J_{Cr} - 0.10\ J_{Ni}$.

Table 2 reports the calculated parameters for the effective Hamiltonian (2). We find a small Ni-ring exchange interaction in all compounds. In particular, J_{iso} is AFM for the two *cis*-compounds **4** and **5**, but significantly stronger in **4** than in **5**, as super-exchange is stronger through pyridine than pyridazine; this is consistent with the variation in the Ni-N bond distance in these two compounds (Table 1). AFM couplings are found in the **6** and **8** variants, wheeras **7** shows a FM and significantly larger value of J_{iso}. This is due to replacement of $CH_3 \rightarrow CF_3$ in the Ni(hfac)$_2$ unit. Figure 3 shows that

Table 1 | Structural parameters for the central Ni coordination site in 4–8

	Cis-compounds		*Trans*-compounds		
	4	5	6	7	8
Bond lengths/Å					
Ni-N	2.02(2)	2.074(7)	2.105(6)–2.122(6)	2.074(9)	2.075(9)
Range Ni-O	2.02(2)–2.025(18)	2.021(6)–2.032(7)	2.013(6)–2.034(7)	2.019(10)–2.034(9)	2.018(8)–2.020(8)
Bond angles/°					
N-Ni-N	92.6(4)	89.9(4)	177.5(3)	180.0	180.0
Range *Cis* N-Ni-O	87.6(8)–91.4(8)	90.6(2)–94.4(3)	85.9(3)–93.1(3)	88.7(4)–91.3(4)	89.6(4)–90.4(4)
Range *trans* N-Ni-O	178.7(9)	178.2(3)	n.a.	n.a.	n.a.
Range *cis* O-Ni-O	87.8(10)–92.3(14)	86.3(3)–88.9(4)	88.4(3)–91.6(3)	88.4(4)–91.6(4)	88.9(4)–91.1(4)
Range *trans* O-Ni-O	176.6(14)	171.0(4)	179.1(3)–179.8(3)	180.0	180.0

Table 2 | Parameters of the Spin Hamiltonian deduced ab-initio. Calculated exchange and zero field splitting parameters of the effective Hamiltonian (2)

Compound	J_{iso}/μeV	J_{an}/μeV	D/meV	E/meV
4	16.1	3.00	−0.32	−0.01
5	1.7	0.23	−0.27	−0.03
6	0.5	0.03	−0.47	−0.06
7	−27.4	−3.00	−0.72	−0.05
8	14.2	2.00	−0.44	−0.02

the overlap between the calculated *d*-like orbitals of the Ni-switch and of the ring is significantly larger in this case, because the $CH_3 \rightarrow CF_3$ substitution leads to a larger delocalization of the orbitals belonging to the Ni-switch. This also explains the intermediate value (in modulus) of J_{iso} found in **8**, in which the substitution has been carried out on only half of the CH_3 groups. These results demonstrate the sophisticated level of chemical control of the magnetic coupling between the Ni-switch and the rings in this family.

Figure 2 shows (black arrows) the z axis direction, obtained by diagonalization of the on-site zero field splitting tensor $\underline{\mathbf{D}}$. We note that this direction is nearly orthogonal to the planes of the two rings for the *trans*-variants, and nearly parallel for the *cis* compounds. The diagonal form of the $\underline{\mathbf{D}}$ tensor gives direct access to the axial and rhombic parameters, D and E, appearing in the effective Hamiltonian (2): we find negative values of D, for all the examined compounds, indicating an easy-axis magnetic anisotropy along the black arrows of Figure 2. By comparing the crystalline environment of the Ni-switch in the different variants, we note a higher rhombicity in **5** and **6** which results in a larger value of E/D calculated for these compounds (see Table 2). In the reference frame diagonalizing $\underline{\mathbf{D}}$, also $\underline{\mathbf{g}}^{Ni}$ is diagonal. We find nearly isotropic g-tensors for all the examined compounds, with $2.11 < g^{Ni}_{\alpha\alpha} < 2.19$, $\alpha = x, y, z$.

Quantum gates with always on magnetic coupling. Since J_{iso} and J_{an} are much smaller than the other terms, the eigenstates of (2) are practically factorized states $|\text{qubits}> \otimes |\phi_{Ni}>$ and to first order the coupling with the Ni ion merely renormalizes the external field felt by the qubits (see Methods). To illustrate the way gates are implemented, we consider two representative examples of *cis*- and *trans*-compounds. Figure 4a shows the calculated level diagram of **5** as a function of the static field. The four low-energy levels labeled $|\alpha, \beta>$ ($\alpha, \beta = 0,1$) (Figure 4a) practically correspond to $|M_1> \otimes |M_2> \otimes |M_{Ni} = -1>$, where $|M_i>$ is the eigenstate of the component of spin i along $\boldsymbol{B}$. Hence, in these states the two rings are effectively decoupled and we can straightforwardly define the computational basis. Single-qubit rotations can thus be implemented by means of uniform resonant magnetic pulses whose duration is chosen in order to obtain a rotation of the desired

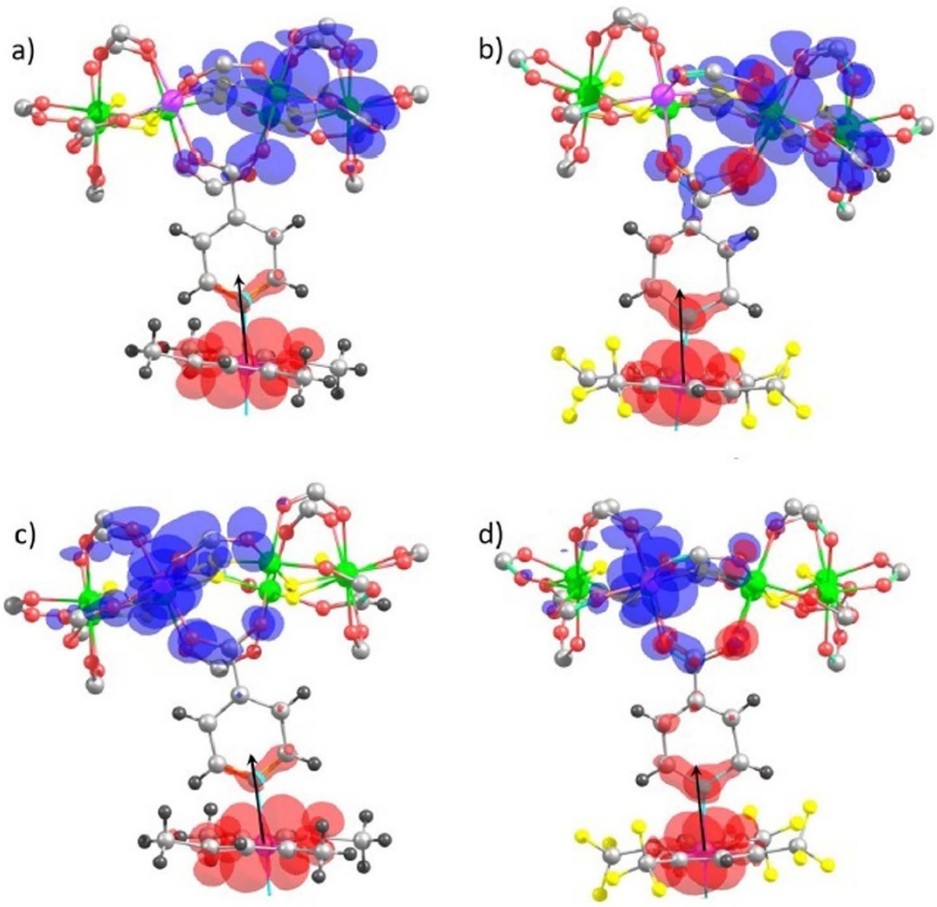

Figure 3 | Chemical control of the ring-Ni coupling. The substitution of CF_3 groups close to the central Ni ion increases the delocalization of its *d*-like orbitals, resulting in a larger overlap with the *d*-like orbitals of $\{Cr_7Ni\}$ rings. This effect is visible in these pictures where only the upper half molecule of Fig. 2 is shown. The surface plots map the modulus of exemplary orbitals providing large contributions to the ring-Ni exchange (red surface: central Ni ion, blue surface: Cr (a,b) and Ni (c,d) ions belonging to the upper $\{Cr_7Ni\}$ ring). (a) and (c) panels refer to the **6** compound, whereas (b) and (d) panels refer to **7**, which displays the largest Ni-ring exchange interaction. In **7** $Ni(hfac)_2$ is the central switch, rather than $Ni(acac)_2$ in **6** (H: dark grey, F: yellow).

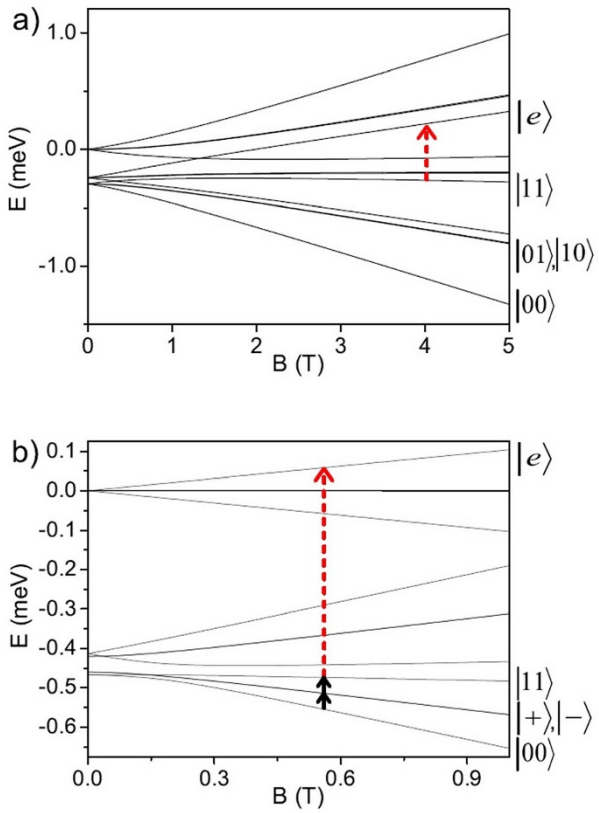

Figure 4 | Level diagram for two representative compounds. (a) Level diagram of **5** as a function of the external magnetic field. The parameters of the spin Hamiltonian (1) are deduced ab-initio. Quantum gates are simulated with a static field of $B = 4\ T$, choosing the direction ($\theta = 65^\circ$ with respect to the Ni easy-axis) to optimize the fidelity. Computational states are defined on the right part of the figure, and the dashed arrow indicates the excitation involved in C-φ. (b) Lowest levels of **8** as a function of the field applied along the Ni easy-axis. The eigenstates correspond to the two qubit states $|00>$ and $|11>$ and to the symmetric and antisymmetic superpositions $|+> \equiv \frac{1}{\sqrt{2}}(|01> + |10>)$ and $|-> \equiv \frac{1}{\sqrt{2}}(|01> - |10>)$. The continuous arrows indicate the transitions involved in the simultaneous rotation of the two qubits.

angle. Since in the *cis*-variants the two rings lie in non-parallel planes, the anisotropy of the $\underline{\mathbf{g}}^i$ tensors of the rings can be exploited to independently rotate each qubit. As an example, we report the calculated time-dependence of the components of the wavefunction $|c_j(t)|^2 = |<j|\psi(t)>|^2$ of compound **5** in a π rotation of the first qubit around the x axis (Figure 5a). In the previous formula, $|j>$ are the two-qubit states belonging to the computational basis and $|\psi(t)>$ is the wavefunction at time t.

Figure 4b reports the calculated field-dependence of the energy levels of the *trans*-compound **8**. In this case the two rings are parallel and it is not possible to individually rotate each qubit with uniform pulses. This implies that these systems can be exploited to simulate only Hamiltonian terms invariant by permutation of the two sites.

The entangling two-qubit gate controlled-φ (C-φ)[35] is obtained (for both *cis*- and *trans*-compounds) by exciting and de-exciting the $|11>$ component of the wavefunction to the state $|e>$ outside the computational basis (see Figure 4), corresponding to a rotation of the Ni-switch state. This allows us to implement a conditional (two-qubit) dynamics because the energy cost of this rotation depends on the states of the two molecular qubits by an amount of the order of J_{iso}. Hence, C-φ can be implemented by a pulse resonant with the gap (dashed arrows in Figure 4), followed by a repetition of the same pulse that brings the state back to $|11>$ (see Figure 5b for **5**) with an additional phase φ. The value of φ is controlled by the phase difference between the first and the second pulse. It is worth to note that the sign of J_{iso} is not important for the feasibility of the scheme.

As a figure of merit for our simulations we consider the gate fidelity, defined as $\mathcal{F} = \sqrt{<\psi|\hat{\rho}|\psi>}$, where $\hat{\rho}$ is the final density matrix induced by the simulated pulse sequence and $|\psi>$ is the target state. Fidelities obtained in the simulation of one- and two-qubit gates for the different compounds are reported in Table 3. For each compound, the direction and magnitude of the applied field are chosen in order to optimize $\mathcal{F}$. These calculations have been performed by initializing the system in a generic superposition of the two-qubit basis states, and by performing rotations of $\pi/3$ around the x axis or controlled-φ gate with $\varphi = \pi$.

In view of designing two-qubits proof-of-principle experiments, we note that the presence of a small rhombic anisotropy allows us to implement high-fidelity quantum gates in *trans*-variants also in small applied fields. Indeed, the resulting anti-crossing in the low-lying energy levels can be exploited to match the two low-energy gaps (continuous arrows in Figure 4b), thus effectively decoupling the two qubits in the computational basis (see Table 3). For all variants we find $\mathcal{F} \geq 99\%$.

The ring-Ni coupling J_{iso} plays a twofold role in determining $\mathcal{F}$: on the one hand large values of J_{iso} ensure large fidelities in the implementation of C-φ gates, on the other hand they give rise to a not-perfect decoupling of the two qubits during rotations (because of the residual second-order coupling, see Methods). Even if J_{iso} is very small in **5** and **6** variants, C-φ can be implemented using oscillating fields of about 10 G. Other variants with larger J_{iso} allow us to employ larger oscillating fields, resulting in shorter gating times. In particular, a value of $|J_{iso}| \gtrsim 2-3\ \mu eV$ allows us to spectrally resolve this transition even with an oscillating field as large as 25 G.

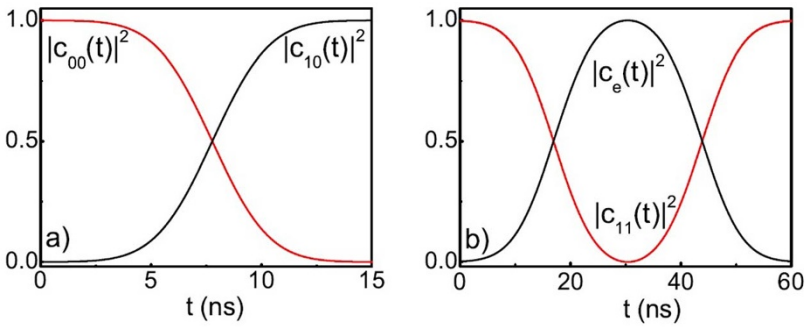

Figure 5 | Simulation of universal quantum gates. Squared absolute value of the components of the system wavefunction $|c_j(t)|^2$ as a function of time, for a single-qubit rotation (a) and C-φ (b). The simulation is performed on **5**, employing a gaussian magnetic pulse $B_\perp(t) = B_{\perp 0} e^{\frac{(t-t_0)^2}{2\tau^2}} \cos\ \omega\ t$, with $B_{\perp 0} = 50$ G (a) and $B_{\perp 0} = 12.5$ G (b). In the variants with larger J_{iso}, the time required for the implementation of C-φ can be substantially reduced by increasing $B_{\perp 0}$.

Table 3 | Fidelity of quantum gates. Fidelities of one- ($\mathcal{F}_R$) and two-qubit ($\mathcal{F}_{CZ}$) gates for each variant of {Cr_7Ni}-Ni-{Cr_7Ni}. The first two columns show the intensity (B) of the static magnetic field and the angle (θ) it forms with the Ni-switch easy axis. The amplitude of the oscillating field employed for CZ ($B_{\perp 0}$) is shown in the last column, while it is always set to 50 G for rotations

Compound	B/T	θ/°	$\mathcal{F}_R$	$\mathcal{F}_{CZ}$	$B_{\perp 0}$/G
4	9.00	13°	99.0	99.9	25
5	4.00	65°	99.9	99.2	12.5
6	1.00	0°	99.9	99.1	10
7	1.17	0°	99.9	99.9	25
8	0.57	0°	99.9	99.9	25

Discussion

Summarizing, we have synthesized a family of {Cr_7Ni}-Ni-{Cr_7Ni} compounds, structurally characterized them and then performed *ab-initio* calculations on all five variants to extract the exchange constants, the zero-field-splitting parameters and the $\underline{\mathbf{g}}$ tensors. Using these results, we have shown that single-qubit rotations and two-qubit gates can be implemented with high fidelities by uniform electromagnetic pulses. Table 3 shows that even if the parameters change significantly in the various compounds, quantum gates can always be implemented. Indeed, the feasibility of these gates only relies on the smallness of $|J_{iso}|$with respect do |D| and not on their precise values.

These systems can thus be exploited to implement quantum simulation algorithms, by decomposing the target time evolution into a sequence of elementary operations[21]. This corresponds to a two-step procedure: i) the time-evolution operator of the Hamiltonian which we want to simulate is decomposed in a product of elementary gates by the well-known Trotter-Suzuki formula; ii) these gates are implemented by a sequence of magnetic pulses as described before. For instance, Figure 6 shows the theoretical results (dots) for the quantum simulation, with the **8** variant, of the oscillations of the magnetization in the prototypical Transverse-field Ising model (TIM), compared with the exact result corresponding to 10 Trotterization steps[3]. The TIM Hamiltonian for N sites is:

$$H_{TIM} = \lambda \sum_{k=1}^{N-1} s_{kz} s_{(k+1)z} + b \sum_{k=1}^{N} s_{kx} \qquad (3)$$

The duration of the pulse sequence implementing the simulation is about 350 ns, significantly shorter than the expected decoherence time. This provides an example of an already feasible proof-of-principle experiment, which would require measuring the magnetization of one of the existing single crystals after the pulse sequence.

An important point in QIP implementations is the potential scalability to a useful number N of qubits. The compounds reported here represent two-qubit units of a potentially scalable quantum simulation scheme. The present switch (the central Ni ion) leads to a non-perfect decoupling of the qubits even in the "off" state. The effect of this small residual interaction increases with N, thus limiting the maximum number of qubits which can be independently rotated. In particular, with the present systems quantum gates can be performed only in short chains with $N \approx 5$–6. This number can be significantly increased, however, by improving the performance of the switch. This could be obtained by modifying the ligand cage of the central Ni ion in order to increase the zero-field splitting and reduce the residual second-order couplings. Alternatively, ions or metal complexes with larger anisotropy could replace Ni as the switch.

In conclusion, the present family of compounds is characterized by the correct hierarchy of parameters to implement sequences of quantum gates and quantum simulation algorithms.

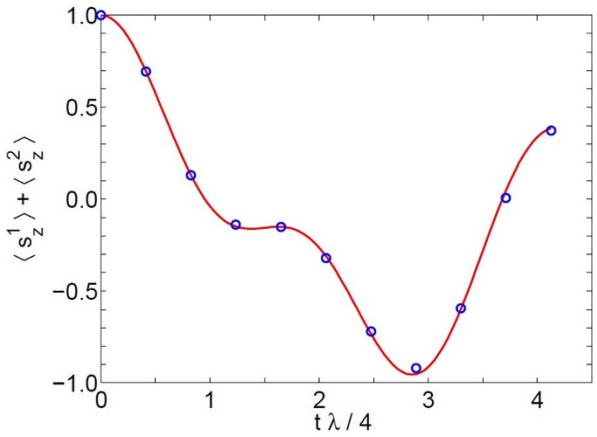

Figure 6 | Simulation of the transverse-field Ising model. Time oscillations of the longitudinal average magnetization $< \sum_i s_z^i >$ in a transverse-field Ising model for the case with $\lambda = 2b$ and $N = 2$ qubits. The spins are parallel at time $t = 0$. The exact result (continuous line) corresponding to 10 trotterization steps is well reproduced by the simulation (dots).

Methods

Experimental. [^{n}Pr_2NH_2][$Cr_7NiF_8(O_2C^tBu)_{16}$] **1** and [^{n}Pr_2NH_2][$Cr_7NiF_8(O_2C^tBu)_{15}(O_2C$-py)] **2** (where HO_2C-py = *iso*-nicotinic acid) was prepared by literature methods[36]. All the other reagents and solvents were commercially available and used as received. Details about the synthetic procedures for [^{n}Pr_2NH_2][$Cr_7NiF_8(O_2C^tBu)_{15}(O_2C$-pd)] **3** (where HO_2C-pd = pyridazine-4-carboxylic acid), [*cis*-(**2**)$_2$-Ni(NO_3)$_2$] **4**, [*cis*-(**3**)$_2$-Ni(hfac)$_2$] **5**, [*trans*-(**2**)-Ni(acac)$_2$] **6**, [*trans*-(**2**)-Ni(hfac)$_2$] **7** and *trans*-(**2**)-Ni(tfac)$_2$] **8** (where acac = acetylacetonate; Hhfac = 1,1,1,5,5,5-hexafluoroacetylacetonate; tfac = 1,1,1-trifluoroacetylacetonate) can be found in the supplementary information.

X-ray crystallography. Structures **4**, **6** and **7** were collected on Diamond light source beamline i19 DLS. Structure **5** was collected on Advanced Light Source station 11.3.1. Structure **8** was collected on a Bruker X8 Prospector 3-circle diffractometer with a copper micro-focus source and an APEX II CCD detector. Structures were solved and refined using SHELX97 and SHELX-2013. CCDC 990653 - 990657 contain the supplementary crystallographic data for this paper. These data can be obtained free of charge from The Cambridge Crystallographic Data Centre via www.ccdc.cam.ac.uk/data_request/cif.

Many-body ab-initio approach. The generalized Hubbard Hamiltonian describing the whole supramolecular system[22] is the following:

$$H = -\sum_{i,i'} \sum_{\sigma,m,m'} t_{m,m'}^{i,i'} c_{im\sigma}^{+} c_{i'm'\sigma} + \frac{1}{2} \sum_{i,i'} \sum_{\sigma,\sigma'} \sum_{m,m'} \sum_{p,p'} U_{m,p,m',p'}^{i,i'} c_{im\sigma}^{+} c_{i'p\sigma'}^{+} c_{ip'\sigma'} c_{i'm'\sigma} + H_{SO} + \mu_B \mathbf{B} \cdot \sum_i (\mathbf{L}_i + 2\mathbf{S}_i) - H_{DC} \qquad (4)$$

where $c_{im\sigma}^{\dagger}$ ($c_{im\sigma}$) creates (annihilates) an electron with spin σ in the Boys orbital m at site i[30]. The parameters $t_{m,m'}^{i,i'}$ are the hopping integrals ($i \neq i'$) or the crystal-field matrix elements ($i = i'$), while $U_{mpm'p'}^{i,i'}$ are the screened Coulomb integrals. The term H_{SO} is the spin-orbit coupling and H_{DC} is the double counting correction, which removes the part of the Coulomb interaction already included in the LDA[22]. In order to reduce the computational effort, calculations are performed by substituting CH_3 groups with H on the rings, according to hydrogen termination technique[26]. However, we did not modify the neighborhood of the Ni-switch. We have checked that this approximation leads only to slight modifications in the extracted single-ring parameters. Calculations have been performed using the structures determined by X-ray diffraction.

Once we have obtained the hopping and the Coulomb integrals of the Hubbard model, by using a canonical transformation, we eliminate charge fluctuations and derive the corresponding low-energy spin model. In this step, it is convenient to work in the basis of crystal-field states, obtained by diagonalizing the on-site matrices $t_{m,m'}^{i,i}$. At all sites the environment of the magnetic ion is approximatively octahedral; thus the crystal-field orbitals split into a lower energy t_{2g}-like quasitriplet and a 1–2 eV higher energy e_g-like quasidoublet. For the systems analyzed in this work, we find that the relevant interactions are described by the spin Hamiltonian Eq.(1), where J_{Ni} and J_{Cr} contain both the screened Coulomb term and the superexchange contributions. The zero-field splitting $\underline{\mathbf{D}}$ and spectroscopic $\underline{\mathbf{g}}^{Ni}$ tensors can be obtained analogously; $\underline{\mathbf{D}}$ is quadratic, while $\underline{\mathbf{g}}^{Ni}$ is linear in the spin-orbit coupling. Our calculations yield the full tensors, and thus we can identify the easy axes of anisotropy.

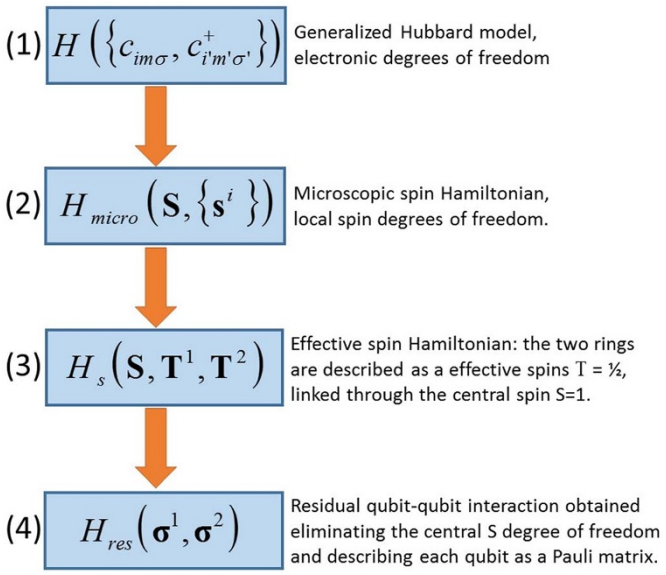

Figure 7 | Scheme of the links between the Hamiltonians. High-energy degrees of freedom are gradually eliminated to reach simpler effective descriptions of the supramolecular system.

Hamiltonians. We provide here (Figure 7) a scheme of the links between the Hamiltonians appearing in the present work. We start from the most fundamental one (H) and we gradually eliminate high-energy degrees of freedom in order to reach an effective description of the system.

(1) H is the generalized Hubbard model of Eq. (4), employed for ab-initio calculations. It is written as a function of fermion operators for localized single-electron Boys orbitals, and it includes many-body effects arising from electron-electron interactions.

(2) By eliminating the small charge fluctuations we deduce the microscopic spin Hamiltonian H_{micro} (Eq. (1) in the main text), written in terms of local spin variables of each magnetic ion.

(3) Since the interactions of each ring with the central Ni^{2+} ion are much weaker than the intra-ring couplings, we can project H_{micro} in the subspace in which the two rings are in the ground doublets $T = 1/2$. In this way we obtain the effective Hamiltonian H_s (Eq. (2) in the main text) which describes the two qubits $\boldsymbol{T}^1$ and $\boldsymbol{T}^2$, linked by the interposed $S = 1$ Ni^{2+} ion.

(4) Finally, we determine the form of the unwanted residual effective ring-ring interaction in the low-energy subspace $M_{Ni} = -1$ (switch in off state), using second-order perturbation theory. The central spin $S = 1$ has been eliminated, leaving an effective qubit-qubit interaction in H_{res}. For instance, if $\boldsymbol{B}$ is along z and assuming for simplicity $E=0$, we obtain a small residual XY interaction between the qubits (apart from a constant term):

$$H_{res} = \frac{\gamma}{2}(\sigma_z^1 + \sigma_z^2) + \frac{\Gamma}{4}(\sigma_x^1\sigma_x^2 + \sigma_y^1\sigma_y^2),$$

where $\sigma_j^{1,2}$ are Pauli matrices referred to each qubit and

$$\gamma = \frac{(J_{iso} - J_{an})^2}{2(D + \mu_B B \Delta g)} - (J_{iso} + 2J_{an}) \qquad \Gamma = \frac{(J_{iso} - J_{an})^2}{(D + \mu_B B \Delta g)}$$

1. Ladd, T. D. Quantum Computers. *Nature* **464**, 45–53 (2010).
2. Feynman, R. P. Simulating Physics with Computers. *Int. J. Theor. Phys.* **21**, 467 (1982).
3. Lloyd, S. Universal quantum simulators. *Science* **273**, 1073–1078 (1996).
4. Georgescu, I. M., Ashhab, S. & Nori, F. Quantum simulation. *Rev. Mod. Phys.* **86**, 153–185 (2014).
5. Aspuru-Guzik, A., Dutoi, A. D. & Love, P. J., Head-Gordon, M. Simulated quantum computation of molecular energies. *Science* **309**, 1704–1707 (2005).
6. Gatteschi, D., Sessoli, R. & Villain, J. *Molecular Nanomagnets* (Oxford University Press: New York, 2007).
7. Sanvito, S. Molecular spintronics. *Chem. Soc. Rev.* **40**, 3336–3355 (2011).
8. Clemente-Juan, J. M., Coronado, E. & Gaita-Arino, A. Magnetic polyoxometalates: from molecular magnetism to molecular spintronics and quantum computing. *Chem. Soc. Rev.* **41**, 7464–7478 (2012).
9. Vincent, R., Klyatskaya, S., Ruben, M., Wernsdorfer, W. & Balestro F. Electronic read-out of a single nuclear spin using a molecular spin transistor. *Nature* **488**, 357–360 (2012).
10. Meier, F., Levy, J. & Loss, D. Quantum computing with antiferromagnetic spin clusters. *Phys. Rev. B* **68**, 134417 (2003).
11. Troiani, F. *et al.* Molecular engineering of antiferromagnetic rings for quantum computation. *Phys. Rev. Lett.* **94**, 207208 (2005).
12. Lehmann, J., Gaita-Arino, A., Coronado, E. & Loss, D. Spin qubits with electrically gated polyoxometalate molecules. *Nature Nanotech.* **2**, 312–317 (2007);
13. Trif, M., Troiani, F., Stepanenko, D. & Loss, D. Spin-Electric Coupling in Molecular Magnets. *Phys. Rev. Lett.* **101**, 217201 (2008).
14. Martínez-Pérez, M. J. *et al.* Gd-Based Single-Ion Magnets with Tunable Magnetic Anisotropy: Molecular Design of Spin Qubits. *Phys. Rev. Lett.* **108**, 247213 (2012).
15. Timco, G. A. *et al.* Engineering the coupling between molecular spin qubits by coordination chemistry. *Nature Nanotech.* **4**, 173–178 (2009).
16. Bertaina, S. *et al.* Quantum oscillations in a molecular magnet. *Nature* **453**, 203 (2008).
17. Moro, F. *et al.* Coherent electron spin manipulation in a dilute oriented ensemble of molecular nanomagnets: pulsed EPR on doped single crystals. *Chem. Commun.* **50**, 91 (2014).
18. Schlegel, C., van Slageren, J., Manoli, M., Brechin, E. K. & Dressel, M. Direct Observation of Quantum Coherence in Single-Molecule Magnets. *Phys. Rev. Lett.* **101**, 147203 (2008).
19. Troiani, F., Affronte, M., Carretta, S., Santini, P. & Amoretti, G. Proposal for Quantum Gates in Permanently Coupled Antiferromagnetic Spin Rings without Need of Local Fields. *Phys. Rev. Lett.* **94**, 190501 (2005).
20. Carretta, S., Santini, P., Amoretti, G., Troiani, F. & Affronte, M. Spin triangles as optimal units for molecule-based quantum gates. *Phys. Rev. B* **76**, 024408 (2007).
21. Santini, P., Carretta, S., Troiani, F. & Amoretti, G. Molecular Nanomagnets as Quantum Simulators. *Phys. Rev. Lett.* **107**, 230502 (2011).
22. Chiesa, A., Carretta, S., Santini, P., Amoretti, G. & Pavarini, E. Many-body models for molecular nanomagnets. *Phys. Rev. Lett.* **110**, 157204 (2013).
23. Carretta, S. *et al.* Quantum oscillations of the total spin in a heterometallic antiferromagnetic ring: Evidence from neutron spectroscopy. *Phys. Rev. Lett.* **98**, 167401 (2007).
24. Wedge, C. *et al.* Chemical Engineering of Molecular Qubits. *Phys. Rev. Lett.* **108**, 107204 (2012).
25. Valiev, M. *et al.* NWChem: a comprehensive and scalable open-source solution for large scale molecular simulations. *Comput. Phys. Commun.* **181**, 1477 (2010).
26. Bellini, V. *et al.* Propagation of Spin Information at the Supramolecular Scale through Heteroaromatic Linkers. *Phys. Rev. Lett.* **106**, 227205 (2011).
27. Cremades, E. *et al.* Theoretical Methods Enlighten Magnetic Properties of a Family of Mn_6 Single-Molecule Magnets. *Inorg. Chem.* **48**, 8012–8019 (2009).
28. Nossa, J. F., Islam;, M. F. & Canali, C. M. First-principles studies of spin-orbit and Dzyaloshinskii-Moriya interactions in the Cu_3 single-molecule magnet. *Phys. Rev. B* **85**, 085427 (2012).
29. For a pedagogical derivation see *The LDA + DMFT Approach to Strongly Correlated Materials*, edited by Pavarini, E., Koch, E., Vollhardt, D. and Lichtenstein, A. Reihe Modeling and Simulation Vol. 1 (Verlag des Forschungszentrum Jülich, Jülich, 2011), Chap. 6.
30. Boys, S. Construction of Some Molecular Orbitals to Be Approximately Invariant for Changes from One Molecule to Another. *Rev. Mod. Phys.* **32**, 296–299 (1960). Boys localization minimizes the spread $|r_1 - r_2|^2$ of the orbitals.
31. A similar procedure, with localized Wannier functions instead of Foster-Boys orbitals, is used to determine magnetic and orbital couplings for strongly correlated transition-metal oxides. See, e.g., Pavarini, E., Koch, E., Lichtenstein, A. I. Mechanism for Orbital Ordering in $KCuF_3$. *Phys. Rev. Lett.* **101**, 266405 (2008).
32. Gunnarsson, O., Andersen, O. K., Jepsen, O. & Zaanen, J. Density-functional calculation of the parameters in the Anderson model: Application to Mn in CdTe. *Phys. Rev. B* **39**, 1708–1722 (1989).
33. MacDonald, A. H., Girvin, S. M. & Yoshioka, D. t/U expansion for the Hubbard model. *Phys. Rev. B* **37**, 9753–9756 (1988).
34. Carretta, S. *et al.* Topology and spin dynamics in magnetic molecules. *Phys. Rev. B* **72**, 060403 (2005).
35. Nielsen, M. A. & Chuang, I. L. *Quantum Computation and Quantum Information* (Cambridge University Press: Cambridge, 2000).
36. Larsen, F. K. *et al.* Synthesis and characterization of heterometallic Cr_7M wheels. *Angew. Chem. Int. Ed.* **42**, 101 (2003).

Acknowledgments

This work has been financially supported by FIRB Project No. RBFR12RPD1 of the Italian MIUR. Calculations were done on the Jülich supercomputer Juropa, grant number JIFF46. E.P. acknowledges financial support from the Deutsche Forschungsgemeinschaft through research unit FOR1346. We thank the EPSRC (UK) for funding and to Diamond Light Source for access to synchrotron X-radiation. The Advanced Light Source is supported by the Director, Office of Science, Office of Basic Energy Sciences, of the US Department of Energy under contract no. DE-AC02-05CH11231. R.E.P.W. is grateful to the Royal Society for a Wolfson Merit Award.

Author contributions

A.C., S.C., G.A. and P.S. developed the scheme for using these systems for quantum information processing and performed numerical simulations and *ab-initio* calculations together with E.P. G.F.S.W, L.C., G.A.T. and R.E.P.W. developed the chemical strategy and synthesized the compounds. S.J.T. performed x-ray experiments.

Additional information

Supplementary information accompanies this paper at http://www.nature.com/scientificreports

Competing financial interests: The authors declare no competing financial interests.

How to cite this article: Chiesa, A. *et al*. Molecular nanomagnets with switchable coupling for quantum simulation. *Sci. Rep.* **4**, 7423; DOI:10.1038/srep07423 (2014).